

Calcium-induced outgrowth of astrocytic peripheral processes requires actin binding by Profilin-1

Dmitry Molotkov^{a,1}, Svetlana Zobova^{a,b,1}, Jose Miguel Arcas^a, Leonard Khiroug^{a,*}

^a Neuroscience Center University of Helsinki, Viikinkaari 4, 00790 Helsinki, Finland

^b Department of Somatological Children's Health, Scientific Research Institute of Medical Problems of the North Siberian Division of Russian Academy of Medical Science, Partizana Zheleznyaka St., 1G, 660022 Krasnoyarsk, Russia

ARTICLE INFO

Article history:

Received 28 January 2013

Received in revised form 12 March 2013

Accepted 16 March 2013

Available online 8 April 2013

Keywords:

Profilin

Actin

Astrocyte

Morphological plasticity

Peripheral processes

Filopodia

Membrane tracing

PAP

Calcium

Photolysis

Uncaging

Cytoskeleton

ABSTRACT

Peripheral astrocytic processes (PAPs) are highly motile structures that are strategically positioned in close proximity to synapses. Long-lasting PAP retraction in hypothalamus is known to alter synaptic transmission [1]. The PAP motility is likely to be actin-based because they are known to contain actin-related proteins such as Ezrin [2]. However, the link between dynamic activity-dependent changes in astrocytic morphology and the synaptic function has not been established experimentally, presumably due to lack of appropriate tools. To selectively suppress activity-dependent morphological plasticity of astrocytes, we developed a bicistronic construct that allows simultaneous tracing and manipulating the morphology of PAPs. The construct is designed for co-expression of (i) the mutant actin binding protein Profilin-1 (abdProf-1) with a single amino acid substitution (H119E) that prevents its binding to actin monomers [3] with (ii) the membrane-targeted morphological tracer LckGFP [4]. Cultured cortical astrocytes transfected with this construct showed abdProf-1 overexpression at a 5-fold level compared to the endogenous Profilin-1. The cells also expressed LckGFP at a level sufficient for precise morphological tracing. We found that photolysis of caged Ca^{2+} induced a pronounced outgrowth of PAPs, which was suppressed by abdProf-1 overexpression in terms of PAP number, growth rate and maximal length. In contrast, the morphological complexity of astrocytes, basal motility of their PAPs and major cytoskeletal structures were not affected by abdProf-1 overexpression. In summary, we identified the actin binding by Profilin-1 as a pivotal mechanism in activity-dependent morphological plasticity of PAPs in cultured astrocytes.

© 2013 Elsevier Ltd. All rights reserved.

1. Introduction

Astrocytes *in vivo* have a very complex 3D structure (reviewed in [5]), which is shaped by their numerous and highly ramified thin peripheral processes [4,6]. These peripheral astrocytic processes (PAPs) form branches of different orders and thicknesses down to submicrometer in size. In order to detect the thinnest ones by means of light microscopy, researchers have relied on membrane staining that highlights PAPs more efficiently than the cytoplasmic one [4]. It has been shown that each astrocyte occupies a distinct spatial domain determined by the spread of its PAPs, and that these domains show very little overlap [6,7].

The majority of PAPs are positioned in close proximity of synapses [8] and are involved in modulation of synaptic transmission and/or plasticity in a variety of ways that include: (i)

ephrin-mediated signaling [9]; (ii) postsynaptic and presynaptic action of ATP released by astrocytes [10,11]; (iii) clearance of glutamate by astrocytes through glutamate transporters [1]; (iv) control of glutamate spillover from synapses and diffusion in extracellular space [12]; (v) N-methyl-D-aspartate (NMDA) receptor co-activation by glia-derived D-serine [13]; (vi) activation of postsynaptic NMDA receptors by glutamate released from astrocytes [14]; and (vii) activation of presynaptic metabotropic glutamate receptors by astrocyte-derived glutamate [15,16].

In addition to functional interactions with pre- and postsynaptic compartments, the perisynaptic PAPs exhibit a high rate of morphological restructuring in a variety of preparations including organotypic hippocampal cultures [4,17] and brain slices [18–20]. During lactation, glial processes are subject to long-term morphological modification in the supra-optical nucleus (SON) of hypothalamus, where retrieval of astrocytic processes affects synaptic properties [1] and increases glutamate spillover [12]. Based on these findings, it is plausible to hypothesize that activity-dependent restructuring of PAPs is a key mechanism in modulation of synaptic function by astrocytes.

* Corresponding author. Tel.: +358 45 635 2270; fax: +358 91 915 7620.

E-mail address: leonard.khirug@helsinki.fi (L. Khiroug).

¹ These two authors have contributed equally to this work.

Several approaches designed to affect astrocytic morphology have been proposed for use in both *in vitro* and *in vivo* models. SON of the hypothalamus in lactating animals provides a classical model for studying the effects of long-term astrocytic retrieval on synaptic properties [1]; however, this preparation does not provide any insight into putative short-term effects of PAP retrieval from synapses. Application of pharmacological agents, such as Latrunculin B in sub-lethal concentrations [21], allows manipulating cytoskeleton motility in an acute manner; however, pharmacological tools lack cell type specificity and are not readily translatable to *in vivo* applications. Ideally, the tool for manipulating short-term PAP plasticity should possess the following features: (i) be genetically encodable, (ii) provide a possibility of selective expression in astrocytes, (iii) allow *in vivo* use, and (iv) specifically affect the activity-dependent plasticity of PAPs (e.g., stimulated outgrowth), rather than their base-level motility.

Morphological plasticity of peripheral extremities in a variety of cell types, ranging from filopodia and lamellipodia in keratinocytes to dendritic spines and presynaptic terminals in neurons, is primarily driven by actin remodeling. Interestingly, despite the widespread assumption that actin treadmilling underlies PAP restructuring [2,17,19], direct evidence of actin presence in PAP is scarce. Nevertheless, it has been shown that PAPs contain a variety of actin-associated proteins, such as ezrin [2,22]. Extensive research on cytoskeleton regulation has revealed a number of actin-binding molecules that regulate remodeling of filopodia and filopodia-like structures. For example, WASP, Myosin X and Fascin are the main regulators of actin dynamics involved in formation and motility of filopodia [23]. In contrast, Profilin-1, Cofilin and Arp2/3 control the dynamic equilibrium of motile actin throughout the cell [24]. All these components of actin-controlling machinery utilize distinct mechanisms, and their activation can shift the dynamic equilibrium either towards net polymerization (Arp2/3 and Profilin-1) or net depolymerization (Cofilin) of actin. Taking advantage of the dynamic nature of actin filaments, one can attempt to selectively manipulate fine morphology and peripheral dynamics without affecting significantly the static morphology of the cell [3,25].

Physiological activation of astrocytes is universally associated with a transient increase in intracellular Ca^{2+} ($[\text{Ca}^{2+}]_i$; reviewed by [26]). To stimulate astrocytes, a variety of receptor agonists, ionophores and other pharmacological agents have been used to increase $[\text{Ca}^{2+}]_i$ via either Ca^{2+} influx or release from internal stores [27–29]. An elegant way to induce a rapid, influx-independent rise in $[\text{Ca}^{2+}]_i$ is offered by photolysis of caged Ca^{2+} [30–33].

Here, we developed a genetically encoded tool allowing both the visualization of astrocytic membrane by means of LckGFP [4] and selective manipulation of stimulated morphological plasticity of PAPs using the actin binding-deficient Profilin-1 (abdProf-1) [3]. By applying this tool in cultured astrocytes in combination with Ca^{2+} uncaging and time-lapse fluorescence microscopy, we found that abdProf-1 expression selectively reduces Ca^{2+} -induced PAP outgrowth, while affecting neither the base level motility nor the general morphology of astrocytes.

2. Results

2.1. Astrocytic fine processes are efficiently traced with LckGFP overexpression

To visualize PAPs with high signal-to-background contrast, we traced plasma membrane using cotransfection of membrane-targeted Lck-EGFP [4] and simultaneously labeled F-actin in cultured astrocytes by overexpression of Lifeact-RFP [34]. An example of highlighted PAPs is shown in Fig. 1. Using the advantages

of tracer expression instead of the post-fixation staining (with e.g. phalloidin), we were able to avoid the cell permeabilization step and preserve the thin membrane structures such as PAPs. We found that both Lifeact-RFP and Lck-EGFP allowed tracing thin astrocytic processes with a high contrast and resolution (Fig. 1A–D). By quantifying co-localization of RFP and EGFP in peripheral processes of cultured astrocytes (Fig. 1E and F), we found that over 95% of PAPs contained F-actin ($95.2 \pm 1.7\%$, $n = 13$ cells). These data confirm that PAPs express high levels of F-actin and have a filopodia-like organization. They further suggest that PAP movements are likely driven by actin-dependent mechanisms. Our observations also demonstrate that both Lck-GFP and Lifeact-RFP are suitable markers for morphological tracing of thin astrocytic processes.

2.2. Simultaneous expression of abdProf-1 and LckGFP using the bicistronic cassette

We constructed a bicistronic cassette for simultaneous expression of the mutated actin-binding protein Profilin-1 (H119E) that contains the single amino acid substitution preventing its binding to actin monomers (abdProf-1) [3] and of LckGFP for tracing astrocytic membranes [4]. Expression of both genes in the cassette is driven by a single CMV promoter. Translation of the first open reading frame encoding abdProf-1 has a Cap-dependent mechanism, while translation of the second open reading frame encoding Lck-GFP is operated by internal ribosome entry site (IRES) (Suppl. Fig. 1A). Since Cap-dependent translation is more efficient compared to IRES-dependent translation, we placed abdProf-1 gene on the first position thus facilitating its high expression, whereas the membrane tracer LckGFP was placed in the second position yielding a lower expression level. We found that even the relatively low IRES-dependent expression of LckGFP was sufficient for precise tracing of PAPs (Fig. 4F₁–F₃).

To be able to trace PAPs without affecting their motility rates, we constructed a control vector where expression of the LckGFP mRNA is driven by CMV promoter and has a Cap-dependent translation mechanism (Suppl. Fig. 1B). This vector facilitates high expression of LckGFP providing a contrast and signal to noise ratio comparable to bicistronic vector (Fig. 4A and D), thus also allowing PAP tracing (Fig. 4C₁–C₃).

To estimate the expression level of abdProf-1 from CMV-profilin-1(H119E)-IRES-LckGFP cassette, we performed immunofluorescence analysis using anti-Profilin antibody on cultured astrocytes 3 days after transfection. This antibody is able to bind both endogenous (non-mutated) Profilin and mutant abdProf-1, thus allowing estimation of the total content of both proteins. By measuring fluorescence intensity levels in transfected (positive for LckGFP) and non-transfected (negative for LckGFP) cells using epifluorescence microscopy, we found that the anti-Profilin labeling level is significantly higher in transfected cells compared to surrounding non-transfected cells ($p < 0.001$, Mann–Whitney test, $n = 12$ cells in each group; Suppl. Fig. 1C–F). The anti-Profilin labeling intensity in transfected cells was on average 6-fold higher than in non-transfected cells (Suppl. Fig. 1F), which allows us to estimate that, in astrocytes expressing CMV-profilin-1(H119E)-IRES-LckGFP cassette, the average molar ratio between endogenous Profilin and mutated abdProf-1 is 1:5. This high ratio allowed us to expect that abdProf-1 will have a clearly measurable effect on Profilin-1-dependent mechanisms in the transfected cells.

2.3. Astrocytic morphology under resting conditions is not affected by abdProf-1

Malfunction of actin-binding proteins potentially may lead to severe changes in cell morphology. To evaluate the effect

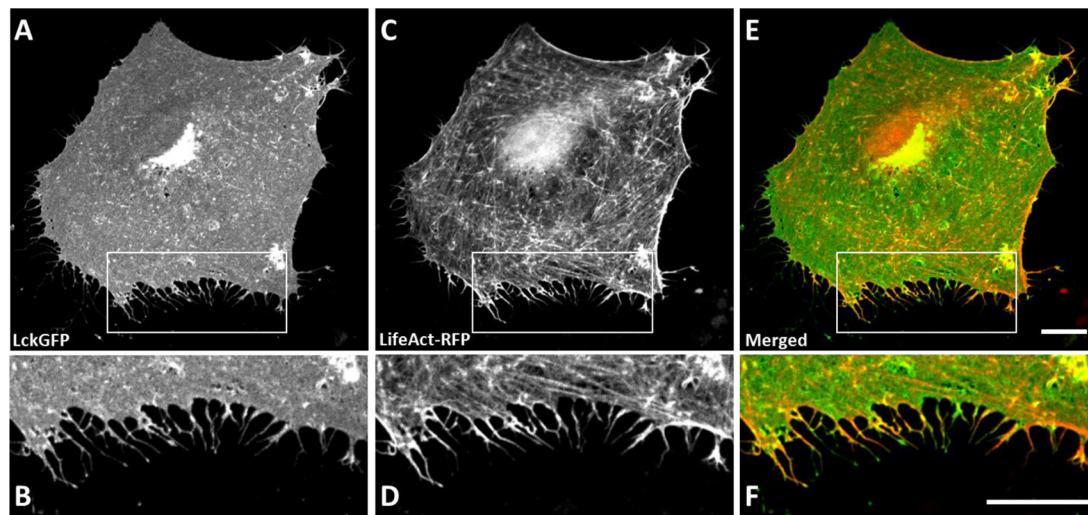


Fig. 1. Filamentous actin (F-actin) traced with LifeAct-RFP overlaps with membrane staining in peripheral astrocytic processes. The LckGFP expression allows tracing of astrocytic membranes (A) and all thin peripheral membrane processes with a high contrast and resolution (B). The expression of LifeAct-RFP in cultured astrocytes facilitates F-actin staining (C), and shows that filamentous actin presents within peripheral astrocytic processes (D). Merging membrane staining (green) with F-actin labeling (red) (E) shows that almost all peripheral astrocytic process contains filamentous actin ($n = 13$ cells) (F). Scale bars are 10 μm .

of *abdProf-1* overexpression on the shape complexity of astrocytes, we compared the traced cell borders in control astrocytes expressing LckGFP (Fig. 2A and C) to those expressing *prof-1*(H119E)-IRES-LckGFP (Fig. 2B and D). The cell edge complexity did not appear different between control and *abdProf-1* expressing cells. To quantify these observations, we measured cell surface area (Fig. 2E) and found that, even though *abdProf-1* expressing cells tended to be smaller (on average by 16%), this difference from control cells was not statistically significant ($p = 0.08$; $n = 50$ cells for control, $n = 54$ cells for *abdProf-1*). In addition, we calculated the average perimeter length (Fig. 2F) and found that it was reduced in *abdProf-1* expressing cells by a degree (16.5%) similar to surface area reduction ($p < 0.001$, Student's t -test; $n = 50$ cells for control, $n = 54$ cells for *abdProf-1*). To evaluate differences in shape rather than size of cultured astrocytes, we normalized perimeter length to surface area and found that the normalized values were equal between control and *abdProf-1* expressing cells ($p = 0.917$) (Fig. 2G). These findings demonstrate that overexpression of *abdProf-1* does not affect the general complexity of cellular morphology, but proportionally decreases both size and perimeter length of astrocytes, thus “scaling” them down by approximately 15%.

2.4. The *abdProf-1* overexpression does not affect stress fiber size

The “down-scaling” effect of *abdProf-1* may suggest that overexpression of the mutant Profilin-1 affects stress fibers, which is the major cytoskeleton structure in cultured astrocytes. To test this hypothesis, we performed fluorescent phalloidin staining and subsequent filament tracing (Suppl. Fig. 3). Phalloidin-based tracing method preferentially highlights the relatively thick actin strands (Suppl. Fig. 3D and H), hence our quantification included primarily the more stable stress fibers rather than the highly motile peripheral actin network elements or microspikes. We found that the traced actin filaments were unaffected by *prof-1*(H119E)-IRES-LckGFP cassette expression (Suppl. Fig. 3E–H) as they were not different from control astrocytes expressing only LckGFP (Suppl. Fig. 3A–D and I; $p = 0.241$; $n = 33$ control cells and $n = 38$ cells expressing *abdProf-1*). This result suggests that overexpression of *abdProf-1* does not affect the size of stress fibers in cultured astrocytes.

2.5. Base-level motility in resting astrocytes is not affected by *abdProf-1*

Next, we tested whether *abdProf-1* overexpression affects basal motility of peripheral structures in primary cultured astrocytes. In order to be able to extract fine cell movements from raw time-lapse microscopy data (Fig. 3A and Suppl. movie 1), we applied a set of digital filters (Fig. 3B; see Section 4 for details) and performed image binarization (Fig. 3C) for each frame in time-lapse image sequences. We calculated the movement of cell edges by measuring the difference in the binarized cell contour between subsequent frames, where the total amount of white pixels in the resulting image represented the total shift of cell edge over a certain period of time (Fig. 3D–F). By using different sampling rates, we were able to detect distinct types of cell movements. Thus, the sampling rate of 0.2 Hz (corresponding to a 5 s inter-frame interval) allows quantification of the relatively fast movements, whereas the sampling rate of 0.02 Hz (50 s interval) reveals the relatively slow movements most likely associated with cell migration rather than spontaneous cell edge fluctuations.

We found that, at both sampling rates of 0.2 Hz and 0.02 Hz, the basal movements of astrocytes expressing *prof-1*(H119E)-IRES-LckGFP was statistically identical to those of control astrocytes expressing only LckGFP (at 0.2 Hz: $n = 17$ for *abdProf-1*, $n = 16$ for control, $p = 0.289$; at 0.02 Hz: $n = 17$ for *abdProf-1*, $n = 18$ for control, $p = 0.880$) (Fig. 3F). Interestingly, the 10-fold increase in sampling interval did not lead to a proportional increase in the total shift of the cell edge, suggesting that there are at least two kinds of movements: (i) back-and-forth fluctuation-like movements revealed by high frequency sampling rate and (ii) slow directional movements detected at the low frequency sampling rate (Fig. 3F). These results demonstrate that overexpression of *abdProf-1* had no effect on the basal motility of cultured astrocytes, including both fast and slow rates of spontaneous movements.

2.6. Photolysis of caged Ca^{2+} stimulates PAP outgrowth

Actin cytoskeleton motility integrates many cellular signaling pathways that can activate or inactivate actin polymerization and trigger peripheral process outgrowth. Since changes in $[\text{Ca}^{2+}]_i$ may serve as a unifying signal for cellular motility, we decided to test

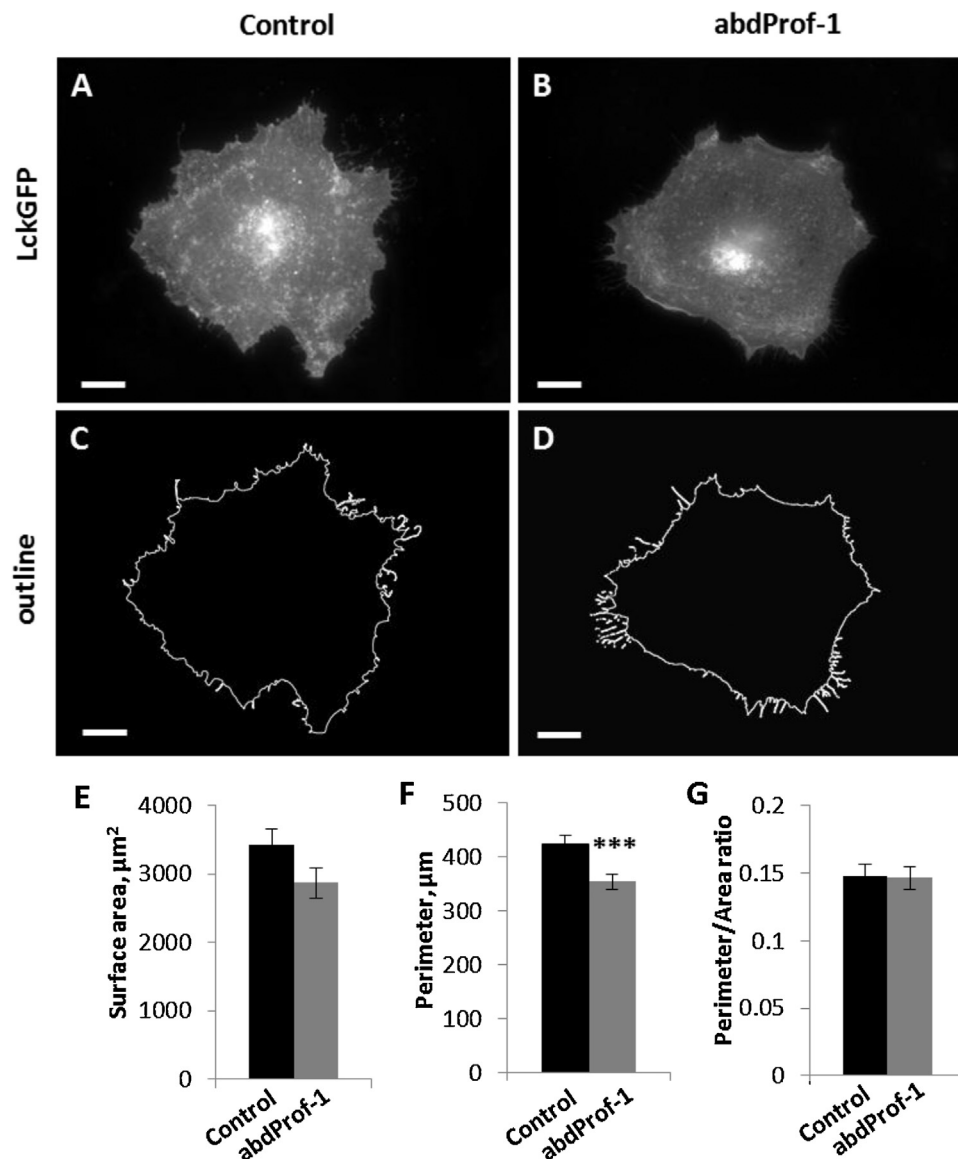


Fig. 2. Effect of *abdProf-1* overexpression on morphological parameters in cultured astrocytes. Representative astrocytic cells and their highlighted outlines expressing CMV-*prof-1*(H119E)-IRES-lckGFP construct (B and D), and mock CMV-lckGFP (A and C). Despite absence of statistical significance, averaged surface area of astrocytes with *abdProf-1* exhibits a tendency to decrease (E). Averaged perimeter length is statistically significant reduced in astrocytes transfected with CMV-*prof-1*(H119E)-IRES-lckGFP construct ($n = 50$ cells for control, $n = 54$ cells for *abdProf-1*; $p < 0.001$, Student's *t*-test) (F). No difference in perimeter length normalized to cell surface area indicates the balanced pattern of observed changes which do not affect cells proportion (G). Error bars indicate SEM. Scale bars are $10 \mu\text{m}$. Significance is designated as *** $p < 0.001$.

if the raise in $[\text{Ca}^{2+}]_i$ will lead to rapid PAPs formation in cultured astrocytes. Using NP-EGTA photolysis as a reliable tool for $[\text{Ca}^{2+}]_i$ manipulation, we found that astrocytes exhibit a rapid outgrowth of peripheral processes in response to flash photolysis of caged Ca^{2+} (Fig. 4A–C₃; Suppl. movie 2). We verified that the UV flash alone, without NP-EGTA loading, did not lead to any significant increase in $[\text{Ca}^{2+}]_i$ (Suppl. Fig. 4B and C) as well as to any rapid morphological changes.

To estimate the actual amplitude of the $[\text{Ca}^{2+}]_i$ rise induced by uncaging, we performed calibration of Fura-2 fluorescence signal using a separate set of cultured astrocytes (Suppl. Fig. 4A). We found that the average $[\text{Ca}^{2+}]_i$ raise in our photolysis experiment had a peak amplitude of 400–600 nM (Suppl. Fig. 4C). The resting $[\text{Ca}^{2+}]_i$ in our astrocytic cultures was around 200 nM (Suppl. Fig. 4A), which is in line with previously reported measurements of $[\text{Ca}^{2+}]_i$ in cultured cortical astrocytes (reviewed by Verkhratsky et al. [35]). Taken together, these results demonstrate that a rapid

0.4–0.6 μM increase in $[\text{Ca}^{2+}]_i$ triggers formation of new peripheral processes in cultured astrocytes.

2.7. Stimulated PAP outgrowth is strongly suppressed by *abdProf-1* overexpression

The main question we addressed in the next set of experiments was whether and to what extent the overexpression of mutated *abdProf-1* affects stimulated PAP outgrowth in cultured astrocytes. We found that astrocytes overexpressing *abdProf-1* were also able to grow PAPs in response to Ca^{2+} elevation but to a lesser extent than control cells (Fig. 4), even though $[\text{Ca}^{2+}]_i$ changes caused by uncaging were similar between *abdProf-1*-expressing and control astrocytes (Suppl. Fig. 4C). Prior to Ca^{2+} uncaging, the PAP densities were the same in both *abdProf-1* and control cells (Fig. 4C₁, F₁ and the first data point in Fig. 4G); at 400 s after the Ca^{2+} stimulation, the PAP density in control cells increased 2-fold ($p = 0.028$, Student's

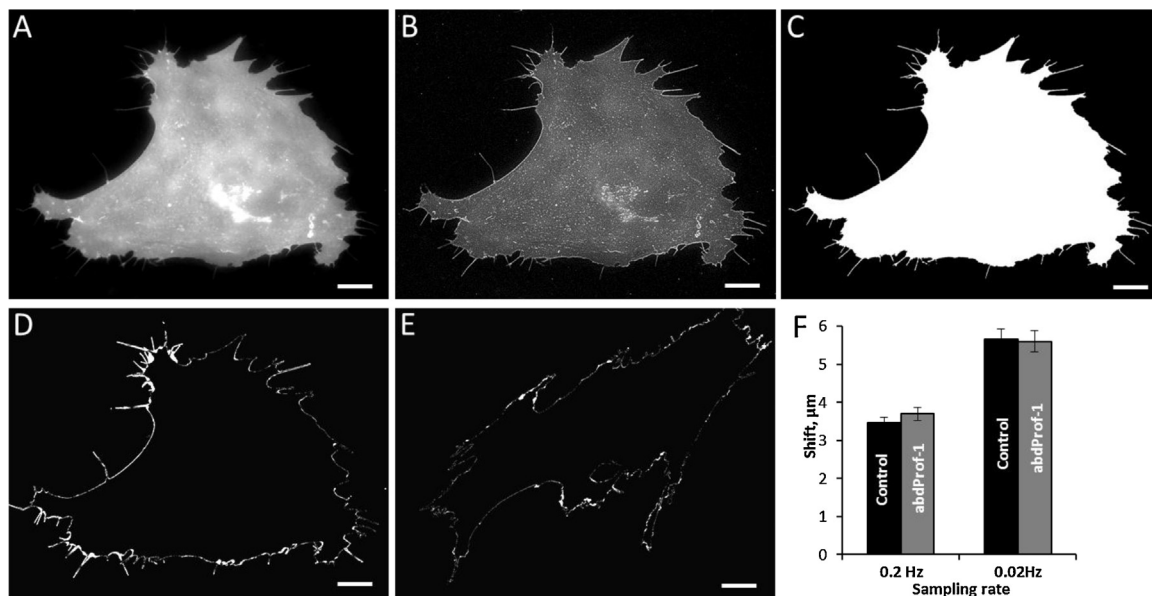


Fig. 3. Overexpression of abdProf-1 does not affect basal kinetics of cell edge in cultured astrocytes. Epifluorescent image of control cell expressing mock CMV-prof-1(H119E)-IRES-LckGFP (A). Application of “top hat” and “sharpen” filters allows highlighting peripheral thin structures (B). Binarization of adjusted image (C). Difference of binarized substacks made with increment 10 (50 s) indicates dynamics of edge movements produced with frequency 0.02 Hz in cells expressing mock (D) and CMV-prof-1(H119E)-IRES-LckGFP construct (E). Total amount of edge movements for fixed period of time (500 s), calculated as area of white pixels normalized on cell perimeter ($n = 35$, Mann–Whitney test), does not differ between control astrocytes and cells expressing abdProf-1 in both selected frequencies (F). Error bars indicates SEM. Scale bars are 10 μm .

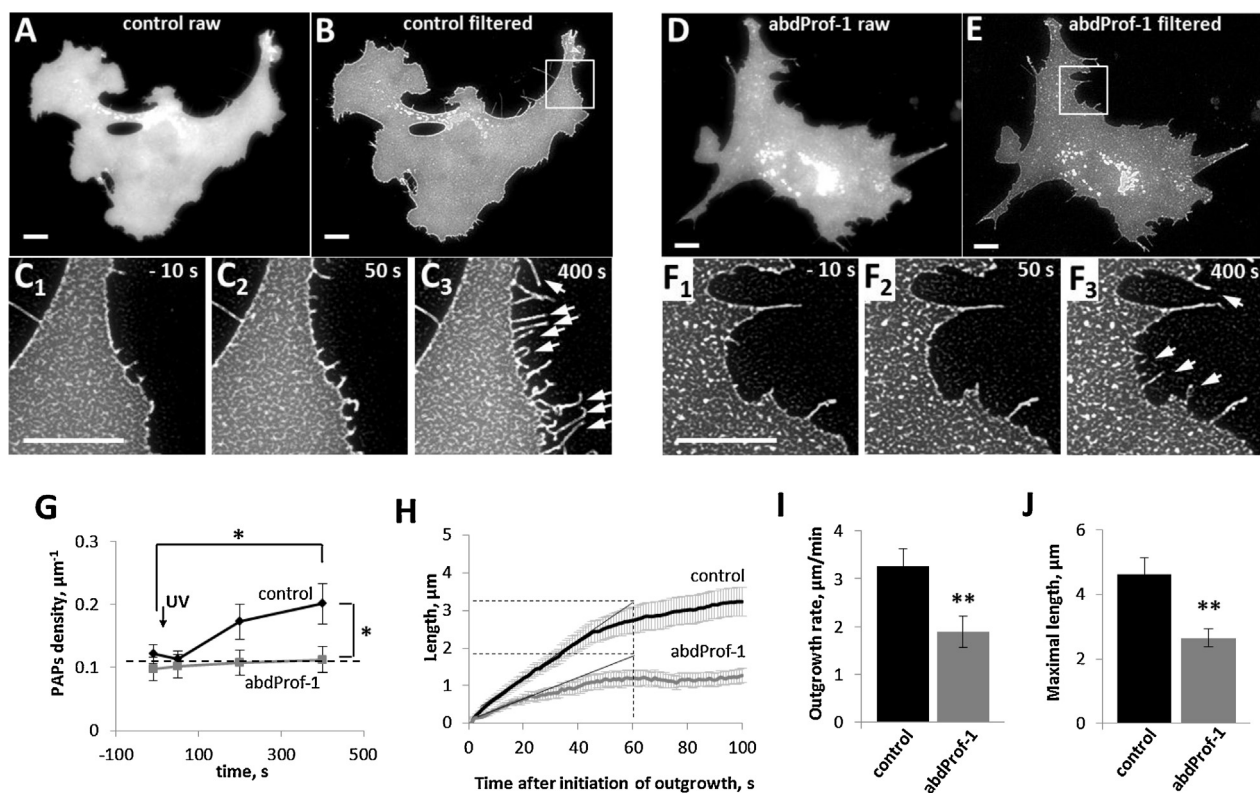


Fig. 4. The rate of Ca^{2+} -induced peripheral astrocytic processes (PAPs) outgrowth is reduced by overexpression of abdProf-1. Representative astrocytic cells expressing CMV-LckGFP (A, B, and C₁–C₃) and CMV-prof-1(H119E)-IRES-LckGFP (D, E, and F₁–F₃) cassettes demonstrate an ability to grow PAPs in a response to Ca^{2+} uncaging (set as zero time point): raw frames within time-lapse movies acquired at 10 s before Ca^{2+} photolysis (A and D), the same images after application of “top hat” and “close” morphological filters (B and E), and time series of filtered fragments at higher magnification taken at selected time points (C₁–C₃ and F₁–F₃). White arrows mark the newly formed PAPs (C₃ and F₃). Total number of PAPs normalized to cell perimeter was an equal in both control and experimental cells prior to Ca^{2+} uncaging; $[\text{Ca}^{2+}]_i$ elevation at 400 s after UV flash induced 2-fold increasing in PAPs density in control cells but not in abdProf-1 expressing astrocytes ($p = 0.028$, Student’s t -test, $n = 15$ cells in each group) (G). Outgrowth kinetics of PAPs in a response to Ca^{2+} stimulation, plotted as average length of PAPs versus time, lapsed from the outgrowth initiation (H). The outgrowth rate during the linear part of the curve (first 25 s) is significantly lower in abdProf-1 expressing astrocytes ($p = 0.007$, Student’s t -test, $n = 35$ PAPs in 12 cells for control and $n = 25$ PAPs in 10 cells for abdProf-1) (I) as well as their maximal length ($p = 0.002$, Student’s t -test, $n = 35$ process in 12 cells for control and $n = 25$ processes in 10 cells for abdProf-1) (J). Error bars indicate SEM. Scale bars are 10 μm . Significance is designated as * $p < 0.05$; ** $p < 0.01$.

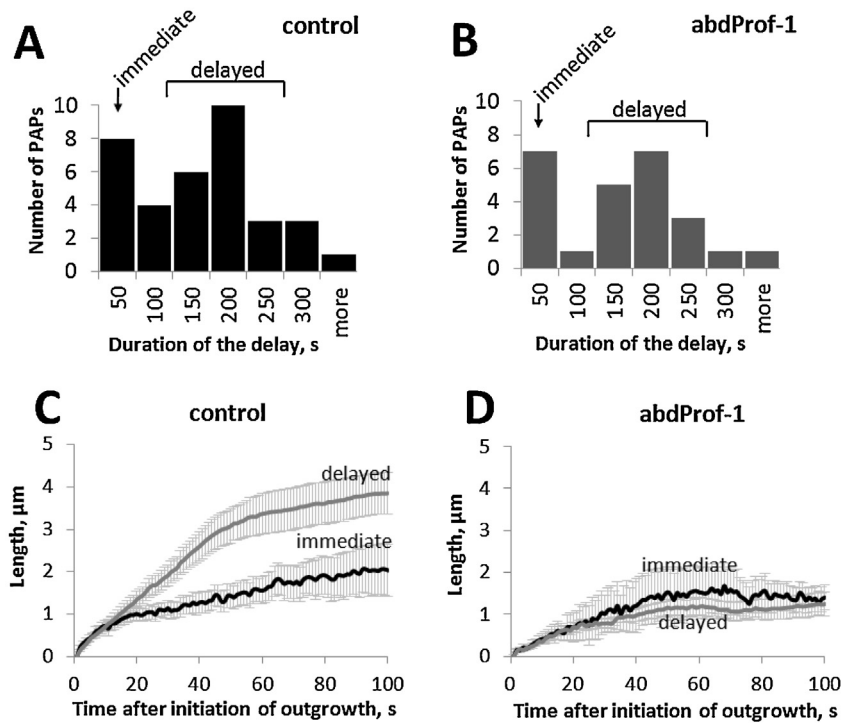


Fig. 5. Distribution of outgrowth initiation delay after Ca^{2+} uncaging was not different for PAPs from control and experimental cells ($\chi^2 = 7.6$, $p = 0.27$; $n = 35$ and 25 , respectively) and allowed to separate PAPs into subgroups, termed “immediate” and “delayed” (A and B). Only delayed PAPs exhibit different outgrowth kinetics in control (C) and abdProf-1 expressing astrocytes (D). Error bars indicate SEM.

t-test, $n = 15$ cells in each group), whereas the abdProf-1 expressing astrocytes showed no increase in PAP density at all (Fig. 4C₃, F₃ and G). Since the PAP outgrowth and retraction are dynamic processes, the images acquired at the 400 s time point represent a snapshot of the dynamic equilibrium state. Thus, the increase in PAP density indicates a shift in the equilibrium towards outgrowth (control cells), while the lack of change in the PAP density is indicative of an unchanged dynamic equilibrium (abdProf-1 expressing astrocytes).

2.8. The rate of Ca^{2+} -stimulated PAP outgrowth is reduced by abdProf-1 overexpression

Despite the dramatically lower number of newly formed peripheral processes in abdProf-1 expressing astrocytes, we set out to determine whether those PAPs that were able to form in abdProf-1 expressing cells had similar properties to those in control cells. We quantified the kinetics of PAP outgrowth in response to Ca^{2+} stimulation and plotted the average length of PAPs against the time lapsed from the outgrowth initiation (Fig. 4H). We found that abdProf-1 expressing cells formed shorter peripheral processes and required longer periods of time for their formation as compared to control cells. We calculated the outgrowth rate during the linear part of the growth curve shown in Fig. 4H (i.e., during the first 25 s after growth initiation) and found that it was significantly lower in abdProf-1 expressing astrocytes compared to control cells ($3.26 \mu\text{m}/\text{min}$ and $1.89 \mu\text{m}/\text{min}$, respectively; $p = 0.007$, Student's *t*-test, $n = 35$ PAPs in 12 cells for control and $n = 25$ PAPs in 10 cells for abdProf-1; Fig. 4I).

Next, we measured the maximal length of newly formed PAPs and found that it was significantly reduced to $2.66 \mu\text{m}$ in abdProf-1 overexpressing astrocytes compared to the average control value of $4.61 \mu\text{m}$ ($p = 0.002$, Student's *t*-test, $n = 35$ process in 12 cells for control and $n = 25$ processes in 10 cells for abdProf-1; Fig. 4J). This result suggests that, besides reducing the PAPs number, abdProf-1

overexpression also slows down the outgrowth and shortens the maximum length of newly formed PAPs after Ca^{2+} stimulation.

2.9. Delayed outgrowth, but not immediate outgrowth, is affected by abdProf-1

By further analyzing the PAP outgrowth dynamics triggered by Ca^{2+} stimulation, we noticed that both control and abdProf-1 expressing astrocytes initiated their PAP growth with a variable latent period after Ca^{2+} photolysis. Plotting the outgrowth initiation delay versus the number of PAPs, we found that both in control (Fig. 5A) and in abdProf-1 expressing astrocytes (Fig. 5B) the PAPs could be separated into two distinct groups according to their outgrowth delay. The first group was termed “immediate” because these PAPs started their outgrowth within the first 50 s after Ca^{2+} uncaging. The second group was designated as “delayed” because these PAPs started growing during the time window from 100 to 250 s after Ca^{2+} uncaging.

For both control and abdProf-1 expressing astrocytes, the histograms of PAP distribution between the immediate and delayed groups had similar bimodal patterns (Chi squared equal to 7.6, $p = 0.27$; Fig. 5A and B). By analyzing the outgrowth kinetics separately for immediate and delayed PAPs, we found that the immediate PAPs showed similar growth kinetics between control and abdProf-1 expressing astrocytes (Fig. 5C and D). In contrast, the kinetics of the growth of delayed PAPs was different in abdProf-1 expressing astrocytes compared to control (Fig. 5C and D). Taken together, the results of Ca^{2+} uncaging experiments suggest a crucial and complex role for actin binding by Profilin-1 in the basic mechanisms of PAP priming and extension.

3. Discussion

The main finding of this study is that cultured astrocytes are able to form peripheral processes in response to $[\text{Ca}^{2+}]_i$ elevation

in a Profilin-1 dependent manner. Selective effect of *abdProf-1* on stimulus-dependent PAPs formation and outgrowth kinetics allow us to propose that PAPs have filopodial nature and are driven by actin cytoskeleton remodeling. This study also provides a novel, validated molecular tool for acute manipulation of activity-dependent peripheral processes outgrowth in astrocytes without affecting basal morphology and motility. This tool can be further applied *in vivo* by means of a proper delivery system. Combined with the *in vivo* two-photon microscopy and/or electrophysiological assays, our tool will be instrumental in elucidating the roles of actin-mediated PAP dynamics in synaptic plasticity within a living brain.

In previous studies, cellular motility has been manipulated primarily by targeting small GTPases known to act upstream of actin-binding proteins. Thus, Wu et al. [36] employed overexpression of photo-activatable small GTPase Rac, while Nishida and Okabe [19] expressed in astrocytes the dominant-negative Rac that decreases PAP movements. Both of these tools rely on shifting small GTPase cascade activation known to be a general actin remodeling regulator that controls primarily lamellipodial rather than filopodial motility [37]. To complement the GTPase-focused approach, we have selected an actin-binding protein Profilin-1 because it supposedly causes less-generalized changes in actin cytoskeleton dynamics as compared to small GTPases.

Astrocytes are generally accepted as important players in synaptic function (reviewed in [38]), and the morphology of their peripheral processes is subject to constant remodeling [5]. The novel molecular tool developed here has an important advantage of selectively affecting actin treadmilling during activity-dependent PAP formation, thus slowing down Ca^{2+} -induced PAP outgrowth without affecting the astrocyte's general morphology or base level motility. Moreover, being genetically encoded, *abdProf-1* in combination with LckGFP can be delivered to a living rodent's brain by either postnatal electroporation [39] or virally mediated gene transfer which offers both time flexibility and astrocyte-specific expression (our unpublished observations). We expect this novel tool to be instrumental in elucidating structure-functional relationship in synaptic plasticity.

Under *in vitro* conditions, astrocytes exhibit very different morphology from that observed in the living brain. In cell culture, these cells are flattened and their complex spongiform three-dimensional structure is largely reduced to two dimensions. Moreover, signal inputs and microgradients observed in cultured conditions are incomparable to those of intact brain. Nonetheless, cultured astrocytes do have filopodia-like processes extending from their peripheral edge, which makes them a suitable model for investigation of molecular mechanisms of PAP formation and motility. We verified that PAPs *in vitro* express actin (Fig. 1) and that their appearance is similar to filopodia, which suggests that their motility is likely based on actin cytoskeleton rearrangement.

Our findings agree with previous reports on PAPs in that astrocytic fine processes likely have filopodial nature [2,22] and may, therefore, share certain features with dendritic protrusions of neurons. It is tempting to cautiously extend the analogy with dendritic spines and propose that each PAP may be viewed as a separate microdomain. As such, PAPs might provide physical constraints for local Ca^{2+} signaling [40], ensure spatially restricted activation of Rho GTPases [41], and enable local RNA interference or mRNA translation [42,43]. Furthermore, we may speculate that, similarly to neuronal filopodia and dendritic spines, PAPs may have distinct sub-regions (or zones) that differ in their actin filament stability and/or regulation mechanisms [44].

Calcium transients are involved in motility regulation of axonal growth cones [45], and local Ca^{2+} uncaging promotes transient extension of filopodia in the growth cone of *Helisoma* snail neurons [46]. We used Ca^{2+} uncaging in primary rat cortical

astrocytes for stimulation of PAP outgrowth because Ca^{2+} photolysis is arguably a more reliable alternative to stimulation of cells with bradykinin [3] or other receptor agonists. We suggest that the uncaging-induced increase in $[\text{Ca}^{2+}]_i$ promotes actin polymerization and PAP outgrowth via calmodulin- and calcineurin-dependent pathways [46,47]. These pathways involve phosphatidylinositol-4,5-bisphosphate as a second messenger for delivering the activation signal to actin cytoskeleton (particularly, to Profilin-1; [48]) as well as to the capping proteins such as gelsolin and CapZ [49]. Thereby, uncaging-induced $[\text{Ca}^{2+}]_i$ rise mimics the integrated downstream effects of a variety of external stimuli received by astrocytes.

Actin cytoskeleton constitutes several structures underlying cell motility, including stress fibers, lamellipodia and filopodia. These actin-based structures differ in their organization and mechanisms regulating their motility [50]. Profilin-1 is one of key players in actin remodeling [24], and its function suppression by overexpression of a mutated *abdProf-1* may, theoretically, affect the dynamics of all types of actin filaments in astrocytes. However, our data demonstrate that expression of the *prof-1*(H119E)-IRES-LckGFP cassette affects only stimulated PAP formation/extension rates (Fig. 4), but has no effect on basal motility of astrocytes (Fig. 3), on general cell shape complexity (Fig. 2) and on stress fibers (Suppl. Fig. 3). While our results are in agreement with those obtained by Takekawa group [3], we can only speculate as to how this specificity of *abdProf-1* action on stimulated motility is realized. Most prominent explanation for this phenomenon is related to the fact that actin turnover in filopodia, lamellipodia and stress fibers is regulated by only partially overlapping pathways [37,51]. Moreover, these structures may have distinct stabilizing mechanisms. For example, stress fibers are stabilized by such proteins as tropomyosin, non-muscle myosins and α -actinin [52,53].

The main functions of Profilin-1 are to catalyze the ADP-to-ATP exchange on actin monomers and to mediate shuttling of G-actin subunits to the F-actin barbed ends [24,54]. Thus, mutant *abdProf-1* has a dual function in the disruption of actin treadmilling: on the barbed end of actin filament it slows the *de novo* polymerization of ATP-bound actin promoted by activation signals, while on the depolymerizing end it promotes stabilization due to its inability to sequester ADP-actin monomers. It is also worth mentioning that a 4-fold increase in Profilin-1 concentration *per se* has been reported to significantly suppress actin-based motility of *Listeria* in an *in vitro* model of actin assembly [54]. In the case of *abdProf-1* overexpression, it is likely that the main factor restricting PAP length and decreasing their outgrowth rates (Fig. 4I and J) is the deficit in ATP-bound G-actin required for rapid polymerization in response to $[\text{Ca}^{2+}]_i$ rise. This notion is further supported by our observation of earlier collapse of PAPs in *abdProf-1* expressing astrocytes (data not shown), which resulted in a net decrease in their length (Fig. 4H and J).

Filopodia building process involves the initiation step followed by the elongation step [51]. Reduction in the number of Ca^{2+} -induced PAPs in *abdProf-1* expressing astrocytes (Fig. 4G) allows us to suggest that one (or both) of these steps may be affected by *abdProf-1* overexpression. Based on our observation of two distinct populations of PAPs, namely "immediate" and "delayed" protrusions (Fig. 5A and B), we propose that there is a certain pool of PAPs that are committed for growth (primed, or pre-formed), which respond rapidly to a $[\text{Ca}^{2+}]_i$ rise. In addition to this pre-formed PAP pool, there may be *de novo* initiated PAPs that start their outgrowth after a certain delay (100–200 s) following the Ca^{2+} stimulation. The observed differences in the growth rate and size between immediate and delayed PAPs, taken together with their differential sensitivity to overexpression of *abdProf-1* (Fig. 5C and D), indicate that immediate and delayed PAPs may constitute two distinct, fundamentally different types of astrocytic processes.

4. Materials and methods

4.1. Plasmid construction

For PCR cloning procedures we used HF Phusion DNA polymerase (Finnzymes, Finland). For DNA digestion and ligation FastDigest restriction exonucleases and Rapid DNA Ligation Kit (Fermentas, Lithuania) were used. The LckGFP [4] sequence from pVETL-LckGFP vector (kind gift from Dr. Steven Green) with flanking restriction sites (BglII and NotI) was cloned by PCR using following primers: tatagatctgccaccatgggctg (forward), taaagcggc-cgcgactctag (reverse). Obtained PCR product was cloned into pJet1.2/blunt vector (Fermentas, Lithuania). Actin binding deficient profilin-1 (H119E) coding sequence (kind gift from Dr. Shiro Suetsugu) with flanking ClaI and XbaI restriction sites was cloned by PCR using following primers: atatcgatagccac-catggccgggtg (forward), cttctagaggtcagtactgggaacgccg (reverse). EMCV internal ribosome entry site (IRES) coding sequence from pEGFP-IRES-KCC2 vector (kind gift from Dr. Claudio Rivera) with flanking restriction sites (XbaI and BglII) was cloned by PCR using following primers: tatctagaatccgcccctctccc (forward), tatagatctttttcaaggaaaaccagc (reverse). PCR products were gel-purified and treated with ClaI, XbaI and DpnI enzymes for prof-1(H119E) or with XbaI, BglII and DpnI for IRES, then fragments were ligated with BglII/ClaI digested pJet1.2-LckGFP vector and whole prof-1(H119E)-IRES-LckGFP cassette was verified by sequencing using pJet2.1 sequencing primers (Fermentas, Lithuania). The cassette was further inserted to a pShuttle-CMV vector [55] (Addgene plasmid #16403) using ClaI/NotI restriction sites in order to obtain CMV-prof-1(H119E)-IRES-LckGFP expression cassette (Suppl. Fig. 1A). Control pShuttle-CMV-LckGFP (CMV-LckGFP) vector was obtained by cloning of LckGFP from pJet1.2-LckGFP to pShuttle-CMV on BglII/NotI sites (Suppl. Fig. 1B). LckGFP sequence then was verified by sequencing. Plasmids for astrocyte transfection were produced in DH5 α *Escherichia coli* strain and were purified using Gene Elute HP midiprep kit (Sigma, USA).

4.2. Cell culture and transfection

Primary cortical astrocyte cultures were prepared from the cerebral cortices of 2–3-day-old Wistar rats. Briefly, cells were dissociated using papain and mechanical trituration in a Ca²⁺- and Mg²⁺-free balanced salt solution (HBSS, pH 7.4), supplemented with 1 mM sodium pyruvate and HEPES. Unless mentioned otherwise, all chemicals were obtained from Sigma. After centrifugation at 1000 rpm for 5 min, cells were suspended in high-glucose Dulbecco's modified Eagle's medium (DMEM; Lonza, Switzerland) supplemented with 10% fetal bovine serum and 25 μ g/mL penicillin/streptomycin (hereafter referred to as complete DMEM). Cells were plated at a density 5×10^4 cells/cm² on 35 mm Petri dish with 14 mm glass bottom microwell (MatTek, USA), pre-treated with Bovine Plasma Fibronectin at 6–6.5 μ g/cm² (Invitrogen, USA) for life cell imaging or poly-L-lysine (1–2 μ g/cm²) for other applications. Cells were grown in 5% CO₂/95% air atmosphere at 37 °C. The day of plating was designated as Day-In-Vitro 0 (DIV0). Medium was changed every 3–4 days. Neurons were preserved in these cultures to maintain a more physiological and complex phenotype of differentiated astrocytes. Cellular composition of the primary cortical culture was characterized with triple staining on 5DIV: anti-GFAP (astrocytes – 52%), anti-TubIII β (neurons – 26%) and DAPI (all nuclei) (Suppl. Fig. 2A).

Cortical astrocytes were transfected with described constructs on DIV2–3 by lipofection according to plasmid DNA transfection protocol. For each MatTek dish, 1 μ L of Lipofectamine 2000 reagent (1 mg/mL; Invitrogen, USA), diluted in 50 μ L of Opti-MEM I with GlutaMAX reduced serum medium (Invitrogen), was added to

0.5 μ g plasmid DNA diluted at the same conditions. Final mix after 30 min incubation at room temperature (RT) was added at the total volume of 100 μ L per dish, with addition of 1 mL of antibiotics-free DMEM, and rinsed after 5 h two times with complete DMEM. Specificity of astrocytic expression was verified with GFAP immunoreactivity (Suppl. Fig. 2B) in 3 separate culture dishes where 39 out of 39, 46 out of 46 and 79 out of 79 LckGFP expressing cells were GFAP positive cells.

4.3. Immunocytochemistry

For immunocytochemical staining, cortical astrocytes were transfected on DIV2–3 with CMV-prof-1(H119E)-IRES-LckGFP plasmid DNA and mock CMV-LckGFP. After 3–5 days, cells were fixed with 4% formaldehyde in phosphate-buffered saline (PBS) containing 4% sucrose for 20 min at RT, rinsed with PBS and permeabilized with 0.2% Triton X-100 in PBS for 10 min at RT. Nonspecific staining was minimized by cells incubation in blocking buffer containing 4% bovine serum albumin (BSA) in PBS with 0.2% Triton X-100 for 2 h at RT. Cells were labeled with the primary and secondary antibodies diluted in PBS containing 4% BSA and 0.2% Triton X-100. For primary antibodies: anti-Profilin-1 antibody (1:200; kind gift from Dr. P. Lappalainen), mouse anti-tubulin-III- β antibody (1:200; MAB1637; Millipore) and chicken anti-GFAP antibody (1:2000; ab4674; Abcam) overnight incubation at +4 °C was used. For secondary antibodies: goat anti-Chicken (A11040, Alexa Fluor 546 conjugated, 1:400; Invitrogen) and goat anti-mouse (A11017, Alexa Fluor 488 conjugated, 1:200; Invitrogen) 2 h incubation at RT was used. Specimens were then mounted in 50% glycerol with DAPI or Fluoromount (Sigma, USA).

4.4. Confocal microscopy

For calculation of the number of PAPs containing actin filaments, cortical astrocytes were cotransfected with membrane tracer LckGFP (kind gift from Dr. Steven Green) and filamentous actin (F-actin) marker LifeAct-RFP ([34]; kind gift from Dr. P. Lappalainen) on DIV2, and fixed on DIV5 as described above. To assess the possible impact of abdProf-1 overexpression on stress fiber formation, cells were transfected with CMV-prof-1(H119E)-IRES-LckGFP and mock CMV-LckGFP on DIV2, fixed on DIV5, permeabilized, stained with Phalloidin-TRITC (P1951, Sigma) 1:1000 at RT for 2 h, and mounted in Fluoromount. Images were investigated using LSM 5 Pascal confocal microscope (Zeiss, Germany) with an oil immersion objective Plan-Apochromat 63x/NA 1.4. The EGFP was excited by 488 nm line of the Ar laser, the fluorescence signal was band-pass filtered at 505–530 nm. For excitation of LifeAct-RFP and Phalloidin-TRITC, we used the 561 nm beam of the He-Ne laser. The emission fluorescence was long-pass filtered at 575 nm.

4.5. Epifluorescence microscopy

For calculation of the perimeter/area ratio, assessment of Profilin-1/abdProfilin-1 level, evaluation of basal cell edge motility, Ca²⁺-induced PAPs outgrowth and Ca²⁺ response in astrocytes, transfected with CMV-prof-1(H119E)-IRES-LckGFP and control CMV-LckGFP plasmids, cells were investigated using inverted Cell-R imaging system (Olympus, Japan), which was equipped with automated wheels for excitation filters and the beam-splitter/emission-filter cubes. Images were collected with a CCD camera (Hamamatsu, Japan). Fluorescence of EGFP was excited at 450/50 nm and collected at 510/50 nm. Alexa Fluor 546 conjugated antibodies were excited at 540 nm and detected at 605/55 nm. Images were taken using oil immersion Olympus PlanApo 60x/NA 1.45 objective. To visualize PAPs for analysis of morphological features, basal cell edge motility, and Ca²⁺-induced PAPs outgrowth

rate, images were acquired at the resolution of 1344×1024 pixels. For assessment of Profilin-1/abdpofilin-1 level and Ca^{2+} response, a lower resolution of 672×512 pixels was employed.

4.5.1. Motility imaging

During all live microscopy experiments, the microscope frame and all optical elements were maintained at 34°C using the temperature control incubator (Solent Scientific, UK). For estimation of basal cell edge motility, astrocytes were transfected on DIV2–3 with CMV-prof-1(H119E)-IRES-LckGFP plasmid DNA and control CMV-LckGFP, and imaged on DIV5–8. During an imaging session, cells were maintained in complete DMEM at 34°C and 5% CO_2 using CO_2 enrichment (Solent Scientific, UK). From each cell, time-lapse movies were recorded with the duration of 500 s, containing 100 frames at 5-s interval.

To visualize Ca^{2+} -induced PAPs outgrowth, fluorescence of EGFP was excited at 500/20 nm and collected at 535/30 nm in order to decrease photobleaching. Basal rate of PAPs outgrowth was detected at sampling rate 1 image per second (totally 30 frames, i.e. 30 s), after Ca^{2+} photolysis images were acquired every 1 s during first 200 s of time-lapse movies (totally 200 frames), and with 10-s intervals for the next 200 s (totally 20 frames).

4.5.2. Ca^{2+} imaging

Ca^{2+} elevations and stimulated PAPs outgrowth were recorded separately due to rapid nature of investigated morphological changes and Ca^{2+} kinetics. For $[\text{Ca}^{2+}]_i$ measurements the Fura-2 imaging technique was used. Cortical astrocytes were loaded by 30 min incubation at 34°C with $4 \mu\text{M}$ Fura-2 AM (Invitrogen, USA) supplemented with Pluronic F-127 (0.025%), in a solution containing (mM): NaCl 127, KCl 3, CaCl_2 2, MgCl_2 1.3, HEPES 20, glucose 10; pH was adjusted to 7.4 with NaOH. After washing out Fura-2 AM, cells were incubated 20 min for de-esterification. Fluorescence of Fura-2 was excited at 380 nm and images were collected at 510 nm. Basal $[\text{Ca}^{2+}]_i$ level was assessed every 500 ms (totally 10 frames). After Ca^{2+} uncaging, 20 frames were recorded at 500 ms interval and subsequent 30 frames were acquired every 3 s to minimize photobleaching. The 340-nm excitation was not used due to limitations imposed by the Olympus PlanApo 60x/NA 1.45 objective. Changes in $[\text{Ca}^{2+}]_i$ were expressed as $\Delta F/F$, where F is baseline fluorescence level, ΔF is the relative change from the base level. For calibration of Fura-2 fluorescent signal F_{\min} values were obtained experimentally using $5 \mu\text{M}$ ionomycin in combination with zero Ca^{2+} , 2 mM Mg^{2+} , and 10 mM Na-EGTA. Mitochondrial Ca^{2+} stores were depleted by application of $5 \mu\text{M}$ oligomycin and $5 \mu\text{M}$ rotenone in order to get rid of the drift in $[\text{Ca}^{2+}]_i$ which occurred during the calibration of Fura-2 fluorescent signal and was likely caused by mitochondrial Ca^{2+} buffering. Thus, depletion of mitochondrial Ca^{2+} stores speeds up the $[\text{Ca}^{2+}]_i$ equilibration process and simplifies the Fura-2 fluorescent signal calibration procedure. The F_{\max} values were determined using a saturating 2 mM Ca^{2+} concentration in combination with $5 \mu\text{M}$ ionomycin. A K_d of 224 nM was used for the calculation [56].

4.5.3. Ca^{2+} photolysis

Transfected cultured astrocytes were loaded with caged Ca^{2+} compound *o*-nitrophenyl (NP)-EGTA AM ester ($10 \mu\text{M}$; Invitrogen) and incubated with $4 \mu\text{M}$ Fura-2 AM (Invitrogen) for 30 min at 34°C in the presence of Pluronic F-127 (0.025%). After washing out (NP)-EGTA AM and Fura-2 AM, cells were incubated 20 min for de-esterification.

An ultraviolet (UV) beam ($<400 \text{ nm}$) from a xenon lamp (150 W) was focused through the oil immersion Olympus PlanApo 60x/NA 1.45 objective to fill the visual field, and the flash duration was set to 200 ms. For each field Ca^{2+} photolysis was applied twice with a 10-min interval: the first flash for activation of signaling cascades

and detection of filopodia outgrowth rate, and the second one for imaging of $[\text{Ca}^{2+}]_i$ response itself. The presence of a reliable Ca^{2+} response to the second UV flash was used as a criterion to determine whether the first UV flash was (i) sufficient for uncaging the compound and (ii) did not induce any irreversible changes in the given cell. In order to verify that the UV flash *per se* does not induce $[\text{Ca}^{2+}]_i$ elevations, the transfected cells ($n=4$) were loaded with Fura-2 without NP-EGTA and exposed to UV flashes of the same intensity and duration as in uncaging experiments. No significant changes in either $[\text{Ca}^{2+}]_i$ (Suppl. Fig. 4C) or motility were observed.

4.6. Data analysis

Images were quantified and processed using ImageJ (available at <http://rsb.info.nih.gov/ij/>), ImagePro 5.1 (Media Cybernetics, USA) and Cell-R (Olympus, Japan) software.

For assessment of F-actin presence in thin peripheral processes, we calculated the percentage of RFP-positive PAPs from the total number of EGFP-positive processes with the width below $1 \mu\text{m}$.

The level of Profilin-1/abdpofilin-1 in control and experimental astrocytes was analyzed by estimation of gray value mean normalized to the average level of fluorescence in cells expressing the mock construct. Background fluorescence was subtracted prior to calculations.

Morphological analysis of the cell coastline perimeter length (P) and surface area (S) was performed using ImagePro 5.1. Prior to the automatic calculation of these parameters, we applied the mask function to the that were previously contrast-enhanced, processed by application of “top hat” and “close” morphological filters, and thresholded. We normalized every value of cell coastline perimeter to the surface area, and used the average P/S ratio as an index of complexity of the cellular morphology.

For evaluation of basal edge motility in astrocytes, each frame within time-lapse movies was first processed by application of morphological filters in ImagePro as described above to enhance contrast and signal to noise ratio, then binarized and background-reduced by removing outliers in ImageJ. For estimation of basal edge movements, time-lapse images were digitally subtracted and a differential image was calculated at two selected frequencies of 0.2 Hz and 0.02 Hz (corresponding to the inter-frame intervals of 5 or 50 s, respectively). The resulting differential image represents the cell edge shift during an inter-frame interval (Fig. 3D and E). The total edge movement during the acquisition of the full time-lapse movie (500 s) was calculated as the area of white pixels normalized to the cell perimeter.

For measurement of PAPs outgrowth rate, each frame within time-lapse movies was filtered in ImagePro by application of “top hat” and “close” morphological filters, binarized and skeletonized in ImageJ (as a result, every outgrowing process was represented as a one-pixel-wide line). For every region of interest containing one selected PAP, we measured the number of white pixels in each frame and plotted it *versus* time. For measurements of outgrowth stimulated by Ca^{2+} uncaging, we plotted the average length of PAPs *versus* time, with the zero point set at the moment of outgrowth initiation. Linear outgrowth rate was calculated for the first 25 s after the growth initiation. Dynamic equilibrium state of PAP density was assessed by calculation of total number of PAP at selected time points: 10 s before Ca^{2+} photolysis, 50, 200 and 400 s after the photolysis.

For stress fibers tracing and length measurement two sets (one representing LckGFP and another representing Phalloidine-TRITC) of confocal images (1024×1024 pixels) were obtained for each cell. Maximum projection image for each confocal z-stack was obtained using LSM Image Browser (Zeiss, Germany). Maximum projection images were converted to 8-bit gray scale and each Phalloidine-TRITC image was masked by corresponding LckGFP

image in ImagePro in order to exclude actin filaments from surrounding untransfected cells. Resulted image was filtered by “top hat”, “close” and “despeckle” filters and then binarized in ImagePro (Suppl. Fig. 3D and H). Total length of all bright objects was measured in ImagePro and normalized on cell surface area.

All data are presented as mean \pm S.E.; n indicates the number of individual cells assessed in immunocytochemical and morphological studies, and number of PAP in the experiments on Ca^{2+} -induced PAPs outgrowth rate. Similar experiments were repeated at least in three culture dishes under the same conditions. Data sets were validated in terms of representativeness of its statistical power. Statistical differences were determined by either t -test for normally distributed data or non-parametric Mann–Whitney U -test of variance, as specified in Section 2. Plots were constructed using MS Excel.

Acknowledgments

Dr. Shiro Suetsugu for cloned actin binding deficient Profilin-1 (H119E) mutant, Dr. Steven Green for LckGFP construct, Dr. Pekka Lappalainen for LifeAct-RFP construct and for anti-Profilin antibody, Dr. Claudio Rivera for pEGFP-IRES-KCC2 plasmid.

Appendix A. Supplementary data

Supplementary data associated with this article can be found, in the online version, at <http://dx.doi.org/10.1016/j.ceca.2013.03.001>.

References

- [1] S. Olier, R. Piet, D. Poulain, Control of glutamate clearance and synaptic efficacy by glial coverage of neurons, *Science* 292 (2001) 923–926.
- [2] M. Lavalie, G. Aumann, E. Anlauf, F. Pröls, M. Arpin, A. Derouiche, Structural plasticity of perisynaptic astrocyte processes involves ezrin and metabotropic glutamate receptors, *Proceedings of the National Academy of Sciences of the United States of America* 108 (2011) 12915–12919.
- [3] S. Suetsugu, H. Miki, T. Takenawa, Distinct roles of profilin in cell morphological changes: microspikes, membrane ruffles, stress fibers, and cytokinesis, *FEBS Letters* 457 (1999) 470–474.
- [4] A.M. Benediktsson, S.J. Schachtele, S.H. Green, M.E. Dailey, Ballistic labeling and dynamic imaging of astrocytes in organotypic hippocampal slice cultures, *Journal of Neuroscience Methods* 141 (2005) 41–53.
- [5] A. Reichenbach, A. Derouiche, F. Kirchhoff, Morphology and dynamics of perisynaptic glia, *Brain Research Reviews* 63 (1/2) (2010) 11–25.
- [6] K. Ogata, T. Kosaka, Structural and quantitative analysis of astrocytes in the mouse hippocampus, *Neuroscience* 113 (2002) 221–233.
- [7] E.A. Bushong, M.E. Martone, Y.Z. Jones, M.H. Ellisman, Protoplasmic astrocytes in CA1 stratum radiatum occupy separate anatomical domains, *Journal of Neuroscience* 22 (2002) 183–192.
- [8] V.I. Popov, N.I. Medvedev, V.V. Rogachevskii, D.A. Ignat'ev, M.G. Stewart, E.E. Fesenko, Three-dimensional organization of synapses and astroglia in the hippocampus of rats and ground squirrels: new structural and functional paradigms of the synapse function, *Biofizika* 48 (2003) 289–308.
- [9] K.K. Murai, L.N. Nguyen, F. Irie, Y. Yamaguchi, E.B. Pasquale, Control of hippocampal dendritic spine morphology through ephrin-A3/EphA4 signaling, *Nature Neuroscience* 6 (2003) 153–160.
- [10] J.M. Zhang, H.K. Wang, C.Q. Ye, W. Ge, Y. Chen, Z.L. Jiang, C.P. Wu, M.M. Poo, S. Duan, ATP released by astrocytes mediates glutamatergic activity-dependent heterosynaptic suppression, *Neuron* 40 (2003) 971–982.
- [11] A. Panatier, M. Vallée, J.Haber, K.K. Murai, J.C. Lacaille, R. Robitaille, Astrocytes are endogenous regulators of basal transmission at central synapses, *Cell* 146 (2011) 785–798.
- [12] E. Syková, Glia and volume transmission during physiological and pathological states, *Journal of Neural Transmission* 112 (2005) 137–147.
- [13] A. Panatier, D.T. Theodosis, J.P. Mothet, B. Touquet, L. Pollegioni, D.A. Poulain, S.H. Olier, Glia-derived D-serine controls NMDA receptor activity and synaptic memory, *Cell* 125 (2006) 775–784.
- [14] P. Jourdain, L.H. Bergersen, B. Bhaukaurally, P. Bezzi, M. Santello, M. Domercq, C. Matute, F. Tonello, V. Gundersen, A. Volterra, Glutamate exocytosis from astrocytes controls synaptic strength, *Nature Neuroscience* 10 (2007) 331–339.
- [15] T. Fiacco, K. McCarthy, Intracellular astrocyte calcium waves in situ increase the frequency of spontaneous AMPA receptor currents in CA1 pyramidal neurons, *Journal of Neuroscience* 24 (2004) 32.
- [16] G. Perea, A. Araque, Astrocytes potentiate transmitter release at single hippocampal synapses, *Science* 317 (2007) 1083–1086.
- [17] M. Haber, L. Zhou, K.K. Murai, Cooperative astrocyte and dendritic spine dynamics at hippocampal excitatory synapses, *Journal of Neuroscience* 26 (2006) 8881–8891.
- [18] J. Hirrlinger, S. Hülsmann, F. Kirchhoff, Astroglial processes show spontaneous motility at active synaptic terminals in situ, *European Journal of Neuroscience* 20 (2004) 2235–2239.
- [19] H. Nishida, S. Okabe, Direct astrocytic contacts regulate local maturation of dendritic spines, *Journal of Neuroscience* 27 (2007) 331–340.
- [20] M.R. Witcher, S.A. Kirov, K.M. Harris, Plasticity of perisynaptic astroglia during synaptogenesis in the mature rat hippocampus, *Glia* 55 (1) (2007) 13–23.
- [21] M.L. Kerber, D.T. Jacobs, L. Campagnola, B.D. Dunn, T. Yin, A.D. Sousa, O.A. Quintero, R.E. Cheney, A novel form of motility in filopodia revealed by imaging myosin-X at the single-molecule level, *Current Biology* 19 (2009) 967–973.
- [22] A. Derouiche, M. Frotscher, Peripheral astrocyte processes: monitoring by selective immunostaining for the actin-binding ERM proteins, *Glia* 36 (2001) 330–341.
- [23] P.K. Mattila, P. Lappalainen, Filopodia: molecular architecture and cellular functions, *Nature Reviews Molecular Cell Biology* 9 (2008) 446–454.
- [24] W. Witke, The role of profilin complexes in cell motility and other cellular processes, *Trends in Cell Biology* 14 (8) (2004) 461–469.
- [25] E.G. Yarmola, M.R. Bubb, How depolymerization can promote polymerization: the case of actin and profilin, *Bioessays* 31 (11) (2009) 1150–1160.
- [26] A. Verkhratsky, J. Rodriguez, V. Papura, Calcium signaling in astroglia, *Molecular and Cellular Endocrinology* 353 (1/2) (2012) 45–56.
- [27] D. Fawthrop, R. Evans, Morphological changes in cultured astrocytes following exposure to calcium ionophores, *Neuroscience Letters* 81 (3) (1987) 250–256.
- [28] A. Cornell-Bell, S. Finkbeiner, M. Cooper, S. Smith, Glutamate induces calcium waves in cultured astrocytes: long-range glial signaling, *Science* 247 (4941) (1990) 470–473.
- [29] C. Chen, J. Chang, W. Chen, Potentiation of bradykinin-induced inositol phosphates production by cyclic AMP elevating agents and endothelin-1 in cultured astrocytes, *Glia* 16 (3) (1996) 210–217.
- [30] Q. Liu, Q. Xu, G. Arcuino, J. Kang, M. Nedergaard, Astrocyte-mediated activation of neuronal kainate receptors, *Proceedings of the National Academy of Sciences of the United States of America* 101 (9) (2004) 3172–3177.
- [31] E. Pryazhnikov, L. Khiroug, Sub-micromolar increase in $[\text{Ca}^{2+}]_i$ triggers delayed exocytosis of ATP in cultured astrocytes, *Glia* 56 (2008) 38–49.
- [32] G. Gordon, K. Iremonger, S. Kantevari, G. Ellis-Davies, B. MacVicar, J. Bains, Astrocyte-mediated distributed plasticity at hypothalamic glutamate synapses, *Neuron* 64 (3) (2009) 391–403.
- [33] M. Koide, A. Bonev, M. Nelson, G. Wellman, Inversion of neurovascular coupling by subarachnoid blood depends on large-conductance Ca^{2+} -activated K^+ (BK) channels, *Proceedings of the National Academy of Sciences of the United States of America* 109 (21) (2012) E1387–E1395.
- [34] J. Riedl, A.H. Crevenna, K. Kessenbrock, J.H. Yu, D. Neukirchen, M. Bista, F. Bradke, D. Jenne, T.A. Holak, Z. Werb, M. Sixt, R. Wedlich-Soldner, Lifeact: a versatile marker to visualize F-actin, *Nature Methods* 5 (2008) 605–607.
- [35] A. Verkhratsky, R. Orkand, H. Kettenmann, Glial calcium: homeostasis and signaling function, *Physiological Reviews* 78 (1) (1998) 99–141.
- [36] Y.I. Wu, D. Frey, O.I. Lungu, A. Jaehrig, I. Schlichting, B. Kuhlman, K.M. Hahn, A genetically encoded photoactivatable Rac controls the motility of living cells, *Nature* 461 (7260) (2009) 104–108.
- [37] T.D. Pollard, G.G. Boris, Cellular motility driven by assembly and disassembly of actin filaments, *Cell* 112 (4) (2003) 453–465.
- [38] G. Perea, M. Navarrete, A. Araque, Tripartite synapses: astrocytes process and control synaptic information, *Trends in Neurosciences* 32 (8) (2009) 421–431.
- [39] D. Molotkov, A. Yukin, R. Afzalov, L. Khiroug, Gene delivery to postnatal rat brain by non-ventricular plasmid injection and electroporation, *Journal of Visualized Experiments* (43) (2010), <http://dx.doi.org/10.3791/2244>.
- [40] T. Yamashita, K. Eguchi, N. Saitoh, H. von Gersdorff, T. Takahashi, Developmental shift to a mechanism of synaptic vesicle endocytosis requiring nanodomain Ca^{2+} , *Nature Neuroscience* 13 (2010) 838–844.
- [41] C.D. Harvey, R. Yasuda, H. Zhong, K. Svoboda, The spread of Ras activity triggered by activation of a single dendritic spine, *Science* 321 (2008) 136–140.
- [42] G.M. Schratt, F. Tuebing, E.A. Nigh, C.G. Kane, M.E. Sabatini, M. Kiebler, M.E. Greenberg, A brain-specific microRNA regulates dendritic spine development, *Nature* 439 (2006) 283–289.
- [43] D.O. Wang, K.C. Martin, R.S. Zukin, Spatially restricting gene expression by local translation at synapses, *Trends in Neurosciences* 33 (2010) 173–182.
- [44] N. Honkura, M. Matsuzaki, J. Noguchi, G.C. Ellis-Davies, H. Kasai, The subspine organization of actin fibers regulates the structure and plasticity of dendritic spines, *Neuron* 57 (2008) 719–729.
- [45] T.M. Gomez, N.C. Spitzer, In vivo regulation of axon extension and pathfinding by growth-cone calcium transients, *Nature* 397 (6717) (1999) 350–355.
- [46] S. Cheng, M.S. Geddis, V. Rehder, Local calcium changes regulate the length of growth cone filopodia, *Journal of Neurobiology* 50 (4) (2002) 263–275.
- [47] H.Y. Chang, K. Takei, A.M. Sydor, T. Born, F. Rusnak, D.G. Jay, Asymmetric retraction of growth cone filopodia following focal inactivation of calcineurin, *Nature* 376 (6542) (1995) 686–690.
- [48] I. Lassing, U. Lindberg, Specific interaction between phosphatidylinositol 4,5-bisphosphate and profilactin, *Nature* 314 (6010) (1985) 472–474.
- [49] T. Takenawa, T. Itoh, Phosphoinositides, key molecules for regulation of actin cytoskeletal organization and membrane traffic from the plasma membrane, *Biochimica et Biophysica Acta* 1533 (3) (2001) 190–206.

- [50] J.V. Small, Getting the actin filaments straight: nucleation-release or tread-milling? *Trends in Cell Biology* 5 (2) (1995) 52–55.
- [51] J. Faix, K. Rottner, The making of filopodia, *Current Opinion in Cell Biology* 18 (1) (2006) 18–25.
- [52] P. Hotulainen, P. Lappalainen, Stress fibers are generated by two distinct actin assembly mechanisms in motile cells, *Journal of Cell Biology* 173 (2006) 383–394.
- [53] M. Nemethova, S. Auinger, J.V. Small, Building the actin cytoskeleton: filopodia contribute to the construction of contractile bundles in the lamella, *Journal of Cell Biology* 180 (2008) 1233–1244.
- [54] T.P. Loisel, R. Boujemaa, D. Pantaloni, M.F. Carlier, Reconstitution of actin-based motility of *Listeria* and *Shigella* using pure proteins, *Nature* 401 (6753) (1999) 613–616.
- [55] T. He, S. Zhou, L. da Costa, J. Yu, K. Kinzler, B. Vogelstein, A simplified system for generating recombinant adenoviruses, *Proceedings of the National Academy of Sciences of the United States of America* 95 (5) (1998) 2509–2514.
- [56] G. Grynkiewicz, M. Poenie, R. Tsien, A new generation of Ca^{2+} indicators with greatly improved fluorescence properties, *Journal of Biological Chemistry* 260 (1985) 3440–3450.